Multiscale Molecular Modelling of ATP-fueled Supramolecular Polymerisation and Depolymerisation

Claudio Perego[1], Luca Pesce[1], Riccardo Capelli[2], Subi J. George[3], and Giovanni M. Pavan*[1,2]

[1]Department of Innovative Technologies, University of Applied Sciences and Arts of Southern Switzerland, Galleria 2, Via Cantonale 2c, 6928 Manno, Switzerland
[2]Department of Applied Science and Technology, Politecnico di Torino, Corso Duca degli Abruzzi 24, 10129 Torino, Italy
[3]Supramolecular Chemistry Laboratory, New Chemistry Unit, Jawaharlal Neru Centre for Advanced Scientific Research, Jakkur, Bangalore, 560064, India

1 Abstract

Fuel-regulated self-assembly is a key principle by which Nature creates spatiotemporally controlled materials and dynamic molecular systems that are in continuous communication (molecular exchange) with the external environment. Designing artificial materials that self-assemble and disassemble via conversion/consumption of a chemical fuel is a grand challenge in supramolecular chemistry, which requires a profound knowledge of the factors governing these complex systems. Here we focus on recently reported metal-coordinated monomers that polymerise in the presence of ATP and depolymerise upon ATP hydrolysis, exploring their fuel-regulated self-assembly/disassembly via multiscale molecular modelling. We use all-atom simulations to assess the role of ATP in stabilising these monomers in assemblies, and we then build on a minimalistic model to investigate their fuel-driven polymerization and depolymerization on a higher scale. In this way, we elucidate general aspects of fuel-regulated self-assembly that are important toward the rational design of new types of bioinspired materials.

*giovanni.pavan@polito.it

2 Introduction

In the course of evolution, Nature has created fascinating materials possessing a complex dynamical behaviour and interesting functional properties such as e.g. dynamic adaptation to the chemical environment, self-healing and stimuli-responsiveness. Many of these materials form through the mechanism of self-assembly, in which fundamental molecular constituents self-recognise and self-assemble via non-covalent interactions to build supramolecular structures, such as micelles, vesicles, fibers, tubes, etc. The dynamics of formation and rupture of these non-covalent bonds among monomers occurs on faster timescales compared to (static) covalent materials, imparting to supramolecular materials an innate dynamic character and peculiar dynamic responsive behaviour[1, 2, 3]. In the last decades, the ability to encode such dynamic properties into artificial supramolecular polymers (SMP) has been developed by supramolecular chemists, and new synthetic self-assembling materials with exquisitely regulated behaviour have been designed[3, 4, 5].

A prominent goal of supramolecular chemistry is to reach a structural and temporal control over self-assembly. This is crucial to design functional materials capable of mimicking the adaptive properties seen in nature. In this perspective, biological materials remain as a major source of inspiration. It is known that many biological structures can assemble, disassemble, change their structure and perform complex functionalities by incorporating, transforming and dissipating energy (e.g. conversion of molecular fuels) in an active communication with the external environment. This allows to obtain structures that operate out-of-equilibrium, or that exist in steady states that are kinetically controlled and regulated by the interaction, conversion and exchange of specific fuel molecules[6, 7, 8]. A relevant example is the cytoskeleton, responsible for cell motility and nutrient trafficking inside the cells [9, 10]. The system is composed of microtubules and actin filaments, that form via transient self-assembly regulated by small molecules such as Adenosine Triphosphate (ATP) and Guanosine Triphosphate (GTP), which act as molecular fuel for the system. The cellular metabolic machinery governs the supply of such molecular fuels, driving the biological functions of the cytoskeleton[11, 12]. Designing artificial materials that form via such regulated self-assembly/disassembly via the supply of specific molecular fuels would be a crucial step to enable temporal and structural control in supramolecular chemistry[13].

Recently, significant advancements towards the design of synthetic fuel-regulated bioinspired materials have been made. For example different groups have designed active SMPs with transient self-organisation, in which polymerisation is controlled by means of kinetic interplay among metastable states in the system [14, 15]. In this context, different strategies have been developed, e.g. by designing dormant oligomers that exhibit a nucleation-elongation self-assembly [16, 17, 18, 19]. A notable case is represented by the system reported in Ref. [20], where living transient SMPs were obtained and temporally controlled through a mechanism reminiscent of Actin self-assembly. In this system, ATP fuel mediates the assembly of specifically engineered monomers with

metal-based receptors (see Sec. 3). In the absence of ATP these monomers form small oligomers, but self-assembly is negligible. On the other hand, when ATP is added, cooperative self-assembly is triggered and the monomers stack into extended fibers (see the cartoon Fig. 1c).

Despite the numerous advancements in this field, the chemical design of biomimetic materials still relies on trial-and-error approaches, which can be very expensive in terms of time and resources. To overcome this issue, mastering the physico-chemical principles of fuel-driven self-assembly is key to direct rational design. However, this requires a molecular-level understanding of the dynamics and of the interactions between the monomers and between the monomers and the fuel molecules, that is most often inaccessible by the experiments. In this perspective, computer modelling holds considerable potential, providing powerful tools to interpret and complement experimental data. In the field of supramolecular polymerisation, molecular dynamics (MD) simulations have been extensively employed [21, 22, 23, 24, 25, 26, 27], allowing to understand crucial aspects of these assemblies that remained inaccessible by experimental techniques. Nonetheless, also computational approaches suffer from limitations when studying the dynamics of SMPs. The behaviour of these intrinsically multiscale systems is controlled on a wide range of temporal and spatial scales, that for example fully atomistic (all-atom, AA) models cannot capture. At the same time, to uncover the crucial details of SMP dynamics requires particle-based models that describe these systems at high sub-molecular resolution. For this reason the *in silico* study of SMPs can take great advantage from simplified molecular descriptions, such as coarse-grained (CG) models, that allow to study larger systems for longer times while still preserving the relevant physico-chemical behaviour of the systems [28, 29, 30, 31], accessing the dynamic behaviour of SMPs at submolecular resolution[32, 33, 34, 35].

Here, focusing as a case study on a recently reported ATP-regulated biomimetic SMP [20], we have employed a multiscale modelling approach to obtain general insights into fuel-driven self-assembly and fuel-regulated disassembly. Starting from an AA description of the system, we first investigated the nature of interactions that dominate these SMPs. Then we translate these insights into a minimalistic CG model that allowed us to simulate the dynamics of self-assembly at much larger scale. We come out with a detailed understanding of the evolution of the system during the fuel-regulated polymerisation and depolymerisation processes. Our models allowed us to elucidate the main physico-chemical factors behind the complexity of the fuel-driven dissipative SMP self-assembly process, which represents an important step towards the design of new biomimetic supramolecular materials.

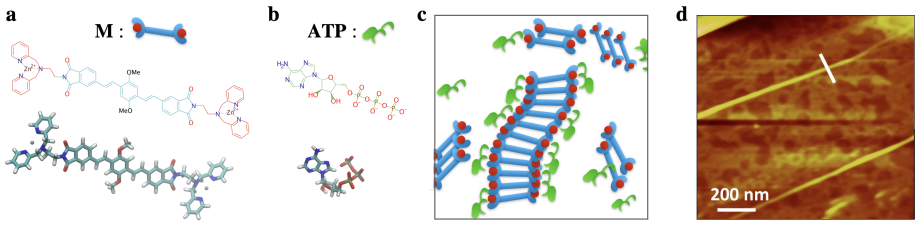

Figure 1: ATP-driven self-assembly of biomimetic supramolecular polymers. a) Chemical structure (top) and AA model (bottom) of the self-assembling monomer **M**. b) Chemical structure (top) and AA model (bottom) of ATP. c) Cartoon representing the fuel-driven self-assembly of **M** triggered by ATP. d) Atomic force microscopy (AFM) of **M**-ATP fibers (dried on highly oriented pyrolytic graphite surface) [20].

3 Results and Discussion

3.1 Atomistic modelling of ATP-stabilised supramolecular polymers

As a representative example of biomimetic, fuel-regulated SMPs, we focus on synthetic monomers (**M**) that self-assemble into long fibers in aqueous solution in the presence of ATP [20]. Monomers **M** consists of an oligo(*p*-phenylenevinylene) (OPV) core functionalised with Zinc (II) dipicolylamine receptors on both ends (Fig.1a). Experimentally, the monomers were proven to interact just sparsely between them in aqueous solution, forming slip-stacked oligomers [20]. However, when ATP is added in solution (Fig.1b), long supramolecular stacks formed via a nucleation-elongation cooperative mechanism (Fig.1d). Reminiscent of the growth of actin filaments, the cooperative self-assembly of **M** SMPs is found to be highly selective towards ATP, and not observed with other fuel molecules, such as adenosine diphosphate (ADP), adenosine monophosphate (AMP) or guanosine triphosphate (GTP). This feature allowed to observe the responsive depolymerisation SMPs via enzymatically triggered ATP hydrolysis [20]. Using these SMPs as a representative case of biomimetic fuel-regulated self-assembling system, here we are interested in tackling fundamental aspects on the molecular mechanisms that control how these assemblies form and exist in exquisitely dynamic regimes, and how these adapt when something changes in the environment (e.g. fuel hydrolysis).

We first built AA models for the monomer **M** and the ATP (see Sec. 5 for more details on the methodologies). We verified that, at the monomeric level, the resulting **M** model remains rigidly extended at $T = 27$ °C in explicit water molecules. We then created a pre-stacked structure composed by 80 monomers, and simulated this SMP in explicit water in two cases: (i) with 320 Cl^- ions to neutralise the +4 charge of each **M**, (ii) with 80 ATP molecules (each of −4 charge). We observe that, while in the first case the assembly is unstable and

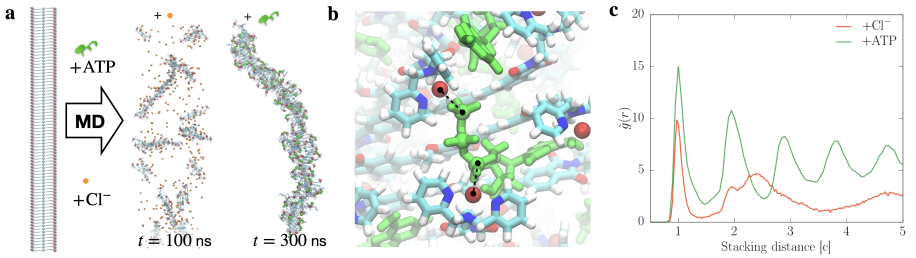

Figure 2: AA simulation of pre-stacked **M**-fibers. a) Representative MD snapshots: the starting configuration, before equilibration, is shown on the left, while on the right the resulting snapshots at the end of the MD simulation are reported. In the presence of neutralising Cl^- ions the fiber dissolves early during the MD run, while in presence of ATP it remains assembled for the whole duration of the simulation (300 ns). b) Zoomed view of a typical arrangement of ATP (in green) in the SMP structure. The multivalent electrostatic interaction between the Zn^{2+} (red spheres) and the ATP phosphate groups (green spheres) is indicated by black dashed lines. c) Core-core radial distribution function $\tilde{g}(r)$ of the two AA-MD systems. $\tilde{g}$ is measured averaging the data calculated from 90 to 100 ns of MD, and it is reported as a function of the inter-core stacking distance (units: $c = 0.38$ nm).

the fiber breaks within the first nanoseconds of MD, in the presence of ATP the aggregate persists as an ordered stack. This is well demonstrated by the radial distribution function of the monomer centres, reported in Fig. 2c: large g(r) peaks at multiples of the inter-stacking distance indicate stacking order, which is substantially preserved in the presence of ATP in the system. Analysing the structure of the ATP-**M** complex we observe that the charged phosphates of ATP steadily interact to the Zn^{2+} ions of the monomers, lowering mutual repulsion between them and stabilising the stack (see Fig.2b). In agreement with previous observations[20], the presence of ATP favours the $\pi - \pi$ stacking of **M** central benzene rings, while in the system without ATP and containing neutralising Cl^- ions the monomer arrange in a slip-stacked configuration (visible in Fig.2a and accompanied by a lower and broader peak at 2.5c in the radial distribution function), losing the long-range order. The results suggest that the driving factor of polymerisation is the interplay of forces between the stacking affinity of the **M** cores and the electrostatic interaction among metal ions and ATP phosphate groups. Data also indicate that the multivalency of ATP is a crucial feature in the self-assembly. However, as already mentioned in the introduction, AA-MD encounters severe limitations in the investigation of supramolecular phenomena, as the relevant timescales of the dynamics are currently out-of-reach within reasonable computational time. To overcome this we rely on the formulation of a CG description, presented in the following.

3.2 CG modelling reveals the effect of fuel concentration on supramolecular polymerisation

Building on the information extracted from the AA-MD (see previous section) and on the experimental evidence [20], we constructed a minimalistic description of the **M**-ATP system. The aim of this minimalistic CG model is to qualitatively reproduce the self-assembly of **M**-ATP by means of a simplified physical picture, retaining only the essential interactions involved in the nature of the system. The model parameters, listed below, were chosen to attain such a qualitative agreement.

The minimalistic CG models of the monomer **M** and fuel are composed of spherical beads, while the solvent is represented implicitly (see Fig. 3a). The solute (**M** and fuel) beads interact by means of Lennard-Jones (LJ) and Coulomb potentials, the LJ radius of all the beads is $\sigma = 0.47\,\mathrm{nm}$. The **M** monomers interactions are mostly localised in 3 interaction centers: 1 core bead (Fig. 3a: in cyan) and 2 charged beads (in red). These are surrounded by 14 weakly interacting beads (transparent CG beads in Fig. 3a). The core beads interact between them with a LJ potential ($\epsilon = 30\,\mathrm{kJ/mol}$), which mimic the core-core affinity in the real system, while all the other beads have a much weaker LJ term ($\epsilon = 0.2\,\mathrm{kJ/mol}$). The red charged CG beads carry a +2 charge representing the metal ions that bind to ATP molecules. In the **M** structure, the CG beads are maintained as in Fig. 3a by means of harmonic bonds, to reproduce the planar geometry of the monomer and to provide a directional screening to the Coulomb interaction. This allowed to observe the formation of fiber-like assemblies during CG-MD in the presence of ATP.

The representation of fuel species is also stripped down to the essential, combining monovalent charged beads that we name $\mathbf{1}^-$ or $\mathbf{1}^+$, as shown in 3a. Also these beads interact via a weak LJ potential ($\epsilon = 0.2\,\mathrm{kJ/mol}$) with the others. In this scheme, ATP is represented by $4 \times \mathbf{1}^-$ connected by harmonic bond and angular potentials, while neutralising Cl^- or Na^+ ions are represented as $\mathbf{1}^-$ or $\mathbf{1}^+$ single beads respectively. As discussed in the following, we have also explored intermediate cases, in which ADP ($3 \times \mathbf{1}^-$ connected beads) or AMP ($2 \times \mathbf{1}^-$ connected beads) are present, and the remaining charge is neutralised by monovalent $\mathbf{1}^-$ ions.

This minimalistic description lowers the computational requirements of MD simulations, significantly increasing the accessible timescales, also for considerably large system sizes. This made it possible to observe the whole process of self-assembly of SMPs starting from the monomeric state. We here present the results of simulations containing $N = 1000$ monomers initially non-interacting and uniformly dispersed in the simulation box. By varying the composition of fuel species in solution we investigated the effect of fuel-to-monomer stoichiometry on the self-assembly process. We tested six cases with different ATP concentration, ranging from 0 to 1.25 times the concentration of monomers [**M**]. The number of monovalent ions in the system was varied accordingly to neutralise the total charge in the system.

The first evidence of ATP-driven self-assembly is shown in Figs.3b and 3c,

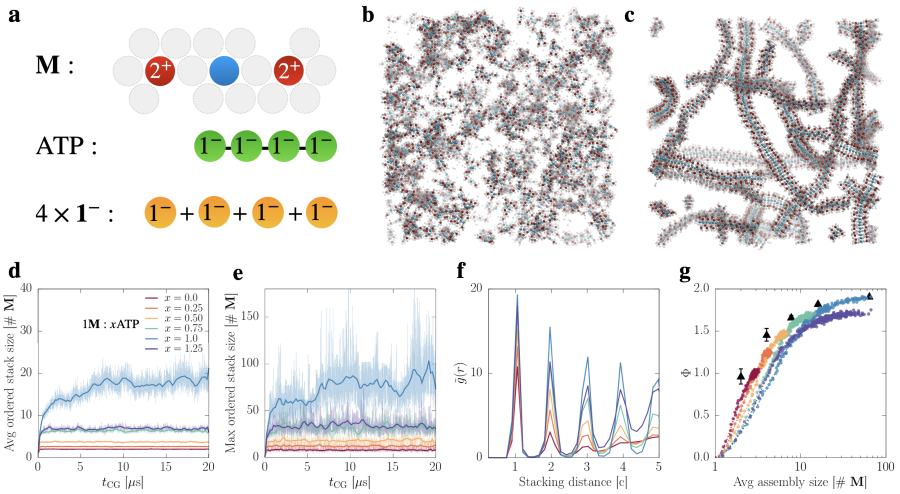

Figure 3: Minimalistic CG model of ATP-driven self-assembly. a) Structures of the different species in the minimalistic model. The monomer **M** (top) is composed of 17 CG beads, a blue core bead (core-core interactions), two +2-charged red beads (Zn^{2+} ions) and 14 screening beads (transparent grey). Below, the scheme of ATP model, composed of 4 connected $\mathbf{1}^-$ charged beads (green), in comparison to the case of monovalent ions (4 non-connected $\mathbf{1}^-$ charged beads). b) Snapshot taken after 20 μs of CG-MD of 1000 **M** monomers with only $\mathbf{1}^-$ fuel ([ATP] = 0). c) same as b) with 1000 ATP ([ATP] = [**M**]). d) Evolution of the average size of ordered stacks at different compositions of ATP. The thick solid line is obtained with Bezier smoothing of the raw data (colored with 0.65 transparency). e) Evolution of the maximum size of ordered stacks. f) Radial distribution function $\tilde{g}(r)$ of **M** cores. The $\tilde{g}(r)$ is measured averaging the data from $t = 19.9\,\mu s$ to $t = 20.0\,\mu s$, and it is displayed as a function of the stacking distance $c = 0.53$ nm. g) Average coordination number Φ of monomer centers as a function of the average size of all assemblies. The black triangles indicate the Φ of pre-stacked assemblies of **M** – ATP. Plots e) f) and g) adopt the same color coding of d).

showing snapshots of two molecular systems, [ATP] = 0 and [ATP] = [**M**], after 20.0 μs of CG-MD. In the absence of ATP the system forms only small aggregates, whereas long ordered fibers are visible in the presence of the multivalent binder (ATP). In the latter case, almost all ATP molecules in the system are contributing to the formation of well-ordered fibers, bridging the CG beads representing the metal ions.

In Figs.3d-g this evidence is explored in a more quantitative way. For sake of clarity we distinguish between two kind of assemblies, the fully ordered stacks, where the monomer cores are parallel and in close-contact from each other, forming flawless fibers, and the generic ones, including also those aggregates presenting defects and disorder (in Sec. 5 we report the methods used to detect, discriminate and characterise assemblies). Simulation data show that the order of the formed assemblies grows with the ATP concentration. This is well demonstrated by the average and maximum size (number of monomers) of the ordered stacks that form during the CG-MD simulations (Fig. 3d and e respectively). The effect of fuel concentration is also evident in terms of average order in the system. This is supported by the radial distribution function ($\tilde{g}(r)$) of the monomer cores (Fig. 3f). The $\tilde{g}(r)$ provides indication on the relative probability of finding monomer cores as a function of the distance between them - large $\tilde{g}(r)$ peaks at core-core stacking distance (c, and multiples of c) identify stable and persistent stacking of cores. Consistently with the data of Figs. 3d,e, $\tilde{g}(r)$ shows that the order is maximised as the [ATP]:[**M**] stoichiometry approaches to 1:1. Interestingly, when the ATP concentration is increased to 1.25[**M**], the size of ordered stacks drops to a level comparable to the 0.75[**M**] case. This suggests that the fuel molecules in excess compete with those bound in fibers, increasing the dynamical exchange of monomers and ATP, enhancing the fluctuations in the aggregate sizes and lowering the persistence of the stacks. Interestingly, we notice that, while the size of ordered stacks is significantly affected when the concentration of ATP is raised from [**M**] to 1.25[**M**] (see Fig. 3g), the average size of generic assemblies reaches similar values (see Fig. S1 and S2 in the Supporting Information (SI)).

Comparing indicators of order and size is useful to understand the mechanism of polymerisation. In Fig. 3g we report the value of the order parameter Φ, namely the average coordination number between the core beads of the monomers, as a function of the average size of generic assemblies[28, 29]. These curves provide indications on the polymerisation pathway as the systems self-assemble. The curves display the typical "cooperative" shape, where the propensity to order increases as larger aggregates are formed. However, we can observe that varying the composition of ATP has an effect on the polymerisation pathway. In particular, as the ratio of [ATP] increases ([ATP] : [**M**] 1:1 in cyan), the system tends to form less ordered assemblies in the early stages of self-assembly, while order emerges into the stacks at a later stage, when larger stacks are formed. On the contrary, at lower ATP concentrations (e.g. [[ATP] : [**M**] 0.25:1 or 0.5:1, in orange and yellow respectively) the stacks reach only shorter sizes, but ordered growth sets in since the first stages of self-assembly. As done recently for other types of SMPs (1,3,5-benzenetricarboxamide, BTA)[29], we

also calculated the average order in equilibrated stacks of $\mathbf{M}-$ATP of different sizes (the black triangles in Fig.3g). These data indicate the ordering Φ that an assembly of a given size would have at the thermodynamic equilibrium, in the absence of kinetic effects. As the ATP concentration is increased, the self-assembly pathways deviate more and more from the equilibrium path indicated by the black triangles. In the early steps of driven self-assembly, the kinetics of the process induces the formation of out-of-equilibrium aggregates, more disordered with respect to equally-sized assemblies at the equilibrium At $\mathbf{M}-$ATP 1:1, the aggregation rate is also increased, determining a higher probability for the monomers to arrange in disordered states before reaching the energetically favoured ordered stacking. The presence of a disorder-to-order transition correlates with the spectroscopic analysis of the assembly process in the real system[20].

Moreover, the trend observed with the change in fuel-monomer ratio is reminiscent of that exhibited by BTA self-assembly as a function of the monomer concentration[29]. Increasing the BTA concentration in water produces a similar tendency to form disordered oligomers, that later rearrange into ordered stacks. On the other hand, at lower concentrations, the polymerisation pathway approaches the degree of order pointed out by equilibrium measurements, similarly to the picture that emerges from Fig. 3g. This analogy suggests that we are detecting a general behaviour, in which a higher self-assembly rate favours the formation of disordered, out-of-equilibrium states.

As reported in Figs. S3 and S4 (see SI), we have also explored the effect of varying the multivalency of the fuel, by simulating the cases [ADP] = [$\mathbf{M}$] and [AMP] = [$\mathbf{M}$] (in both cases the necessary amount of $\mathbf{1}^-$ beads - counterions - was introduced to neutralise the total charge). These results show that the self-assembly process is strongly selective for ATP, leading on average to significantly smaller assemblies in presence of ADP or AMP. Also in this case, the polymerisation pathways reveal that a higher propensity to aggregation corresponds to a more accentuated disorder-to-order transition.

3.3 A deeper view into fuel-driven supramolecular polymerisation

From the previous analysis it is clear that the self-assembly of CG $\mathbf{M}$ monomers is strongly selective for ATP (tetravalent fuel), and that the process occurs on average by passing through disordered oligomers that later reorganise into ordered stacks, acting as nuclei for the elongation of much longer aggregates. However, monitoring average quantities in the self-assembling system does not reveal all the details of the polymerisation process. For example, it would be interesting to assess if the longest stacks grow in solution via fusion of rather static oligomers/fragments or via subtraction of monomers extracted from the smaller, less stable aggregates, or through a combination of different mechanisms.

To gain further insights on the process of fiber formation we focus on the [ATP] = [$\mathbf{M}$] case, and perform the following study: we select one of the longest stacks that is formed late during the CG-MD simulation, and we retrace the

evolution of its forming monomers back in time. In Fig. 4a we show 4 representative snapshots of this aggregate evolution, which reaches its maximum size after $t_{CG} = 17.5\,\mu$s. Qualitatively, the dynamics of the system during growth is clear, as we observe that the red monomers/oligomers, that in the later stages compose the selected fiber (Fig. 4a,right), were part of several different stacks earlier during the simulation. This means that molecular exchange into/out of the stacks is present during self-assembly. This is more quantitatively assessed in Fig. 4b, where we report a cluster analysis of the 182 monomers composing the largest red fiber, which measures the size of the constitutive assemblies in time. We observe that, along the CG-MD run ($20\,\mu$s), the molecules take part in different stacks, showing how monomers, oligomers and relatively long segments are in a continuous exchange, while over time the largest sizes tend to prevail. This is a typical consequence of cooperative growth, which can be directly observed with this minimalistic model.

To deeper investigate the dynamicity of self-assembly, we assessed the evolution of the size distribution of assemblies, again in the [ATP] = [**M**] case (Figs.4b and c). We observe a non-trivial kinetics, in which smaller oligomers (e.g. in red, orange and yellow) leave gradually the way to larger and larger assemblies. Intermediate size populations are transiently dominant at some stage of the MD run (e.g. green, light blue), before being "consumed" by the presence of larger, more stable stacks (dark blue, purple). As a consequence, the emergence of longer fibers exhibits a lag-time, that can be correlated with the lag-time observed in the spectroscopic measurements of **M** − ATP polymerisation [20]. We performed the same analysis also for the other simulated cases (see SI, Figs. S5,S6), observing that lower ATP concentration or lower fuel valency (ADP and AMP cases) determines a faster exchange of monomers and oligomers between the aggregates. As a result, in all the systems of Figs. S5,S6, a stationary distribution of sizes is reached, while this is not the case in Fig.4b, where the dynamicity of the system is slowed down by the persistence of longer and more stable stacks, that tend to attract the free oligomers present in solution. Interestingly, also the [ATP] = 1.25[**M**] case shows a higher dynamicity than the [ATP] = [**M**] case, as the competition between the ATP molecules in excess increases the exchange rate of monomers in the system.

3.4 Driven Disassembly

In analogy with the case of actin, the selectivity towards ATP is a crucial feature for the bioinspired behaviour of **M** monomers, enabling the temporal control of self-assembly by means of ATP hydrolysis to ADP. In the previous sections we have demonstrated that our minimalistic model is capable to display such a selective self-assembly, driven by the multivalency of the fuel and its stoichiometry vs. the monomers in the system. As a next step, we employed our CG model to investigate the fiber disassembly upon ATP hydrolysis. We again focused on the system that assemblies most efficiently, namely the [ATP] = [**M**] case. After $t_{CG} = 9.79\,\mu$s the largest ordered stack (of 202 monomers) is detected. We selected this configuration as the starting point of this study and statically

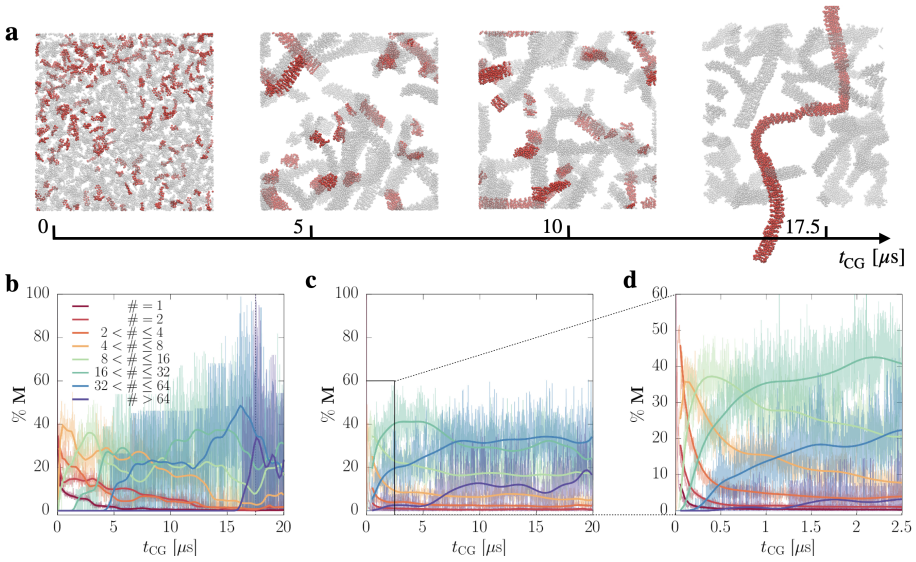

Figure 4: Evolution and growth of ordered assemblies in the [ATP] = [**M**] system. a) Snapshots of **M** configurations taken along 20 μs of CG-MD. The monomers colored in red self-assemble to form a stack of maximum size 182 at $t = 17.5\,\mu$s of simulation. In the last snapshot, to display the extended aggregate (i.e. an infinite fiber), the periodic images of assembled monomers are partly shown. b) Clustering evolution of the monomers that form the aggregate highlighted in a. The thick solid lines represent the exponential moving average (smoothed with Bezier algorithm) of the raw data (colored with 0.65 transparency). The dashed vertical line indicates the time $t_{CG} = 17.5\,\mu$s, at which all the monomers are assembled. c) Fraction of monomers belonging to stacks of a certain size (or range of sizes) plotted vs. simulation time. d) Zoomed view of the first 2.5 μs of c).

converted all ATP molecules to ADP+$\mathbf{1}^-$ (by removing the explicit bond between the third and the fourth $\mathbf{1}^-$ beads in the ATP model). We then restarted the CG-MD simulation and studied the evolution of the system. In Fig. 5a we follow the disassembly of the largest aggregate (in red). After the ATP hydrolysis, the multivalent nature of the fuel is reduced and the fiber swiftly depolymerises into smaller oligomers. Rapidly, the monomers belonging to the initial stack distribute among a new population of assemblies. In Figs.5b and c we note that the system responds very rapidly to the stimulus (hydrolysis), with an abrupt drop of the average order parameter Φ and of the maximum stack size in the system. Such a fast response is due to the dynamicity of the system with ADP+$\mathbf{1}^-$, that soon reaches a stationary state (green data in Figs.5b and c). The fuel cleavage is repeated after 5 μs, converting the ADPs to AMP+$\mathbf{1}^-$, and then again after 10 μs lowering all the fuel population to $\mathbf{1}^-$ beads (see the cartoon in Fig. 5b). Also in these subsequent hydrolysis steps the system shows a swift adaptation to the fuel conversion, especially in terms of average behaviour, while the maximum size of ordered stacks (Fig. 5c) is affected to a lower extent.

Analysing the size population of the system (Fig. S7a) we observe also an abrupt change in the monomer distribution among different stack sizes. This behaviour shows clearly how the system dynamicity increases after the first cleavage (ATP-to-ADP) and how the stability of different aggregates is impaired by the loss in fuel multivalency. In Fig. 5d we report the clustering evolution of the 202 monomers highlighted in red in Fig. 5a, i.e. the size of stacks formed by these selected molecules. The plot reveals the timescale of the monomers redistribution. After the cleavage event, these are rapidly spread among, and reincorporated into, all the aggregates in the system (see also the snapshots of Fig. 5a).

Similarly to what done for polymerisation, it is interesting to analyze the pathway of depolymerisation. Again this is represented by the variation of Φ as a function of the average aggregate size (Fig. 5e), following to the first hydrolysis step. We notice that the system depolymerises along a different pathway with respect to that travelled during polymerisation. In fact, depolymerisation is initially accompanied by a decrease of stacking order Φ, as numerous defects are formed along the fibers right after the fuel hydrolysis (see e.g. the second snapshot of Fig. 5a). Then, the depolymerisation pathway crosses the polymerisation pathway, as the system moves towards the stationary state associated to [ADP] = [$\mathbf{M}$]. The density of points in the colored trajectories of Fig. 5e are representative of the rate of the evolution of the system. In particular, sparse points show that the system is changing very fast in time, while regions dense of points identify a static behaviour of the system, which persists over time in a given state. This shows that the most drastic effect on the assemblies is that produced by the conversion of ATP into ADP, while further cleavages are in comparison less destabilising. Again we observe that a quick change in the system (ATP-to-ADP conversion) pushes the system toward pathways characterised by more disordered states (green circles). The depolymerisation pathway crosses the polymerisation pathway at an average assembly size of 10, while be-

low this threshold the effect on the assemblies is less evident, and the system approaches thermodynamic equilibrium states (black triangles). In Fig. S7b we also report the behaviour of Φ as a function of the maximum size of aggregates, showing how the latter fluctuates heavily upon fuel conversion, at least after the first event of hydrolysis.

4 Conclusions

In this paper we have presented a computational study of fuel-regulated self-assembly process observed in the $\mathbf{M}-$ATP system presented in Mishra *et al.* [20]. We adopted a multi-scale approach, starting from a fully atomistic molecular model of the $\mathbf{M}$ monomer and of the ATP fuel. Our AA-MD simulations were useful to clarify the main factors contributing to the stability of SMPs in presence of an ATP-rich environment. The fuel molecules bridge the zinc-functionalised arms of the monomers, increasing the affinity of the latter to π-π stacking. As a result, ATP stabilises the assemblies, which on the contrary break apart in absence of fuel molecules. These outcomes were found in agreement with the previous simulations presented in Ref. [20], providing insights that cover larger temporal and spatial scales.

We then proposed a CG, minimalistic model that reduces to the essential the interaction involved in the formation of these SMPs. The simplicity of the model allowed us to explore the behaviour of large systems (1000 monomers) for relatively long timescales ($20\,\mu$s), making it possible to observe the dynamics of self-assembly with sub-molecular detail. The reported CG-MD simulations exhibited a biomimetic self-assembly of the monomers in presence of ATP fuel, and demonstrated a strong selectivity towards a $1:1$ monomer-to-fuel stoichiometry. Also the multivalency of the fuel was shown to be crucial for the capability of forming long, ordered fibers. This selective behaviour is in qualitative agreement with the results of Ref. [20] and with the mechanism observed in the regulated assembly of biological systems such as actin filaments. Our simulations demonstrated that fuel-driven self-assembly is the result of a subtle interplay between the electrostatic attraction of charged groups and the stacking affinity of the assembling monomers. Moreover, the multivalency and stoichiometry of fuel are outlined as controlling parameters of the reaction, enlightening possible directions for the development of new materials.

We have also provided insights on the specific features of the self-assembly mechanism, showing the cooperativity of growth, and the tendency of aggregate far from the equilibrium, with the formation of disordered assemblies that acquire order in a successive stage. We presented an extensive investigation of the assembly dynamics, by a detailed cluster analysis of the trajectories, which revealed a complex kinetics in the evolution of the aggregate sizes. The data demonstrate a great dinamicity of the process, in which monomers and oligomers continuously exchange among aggregates, favouring the formation of larger and larger SMPs.

With the proposed model we investigated the disassembly of SMPs as well,

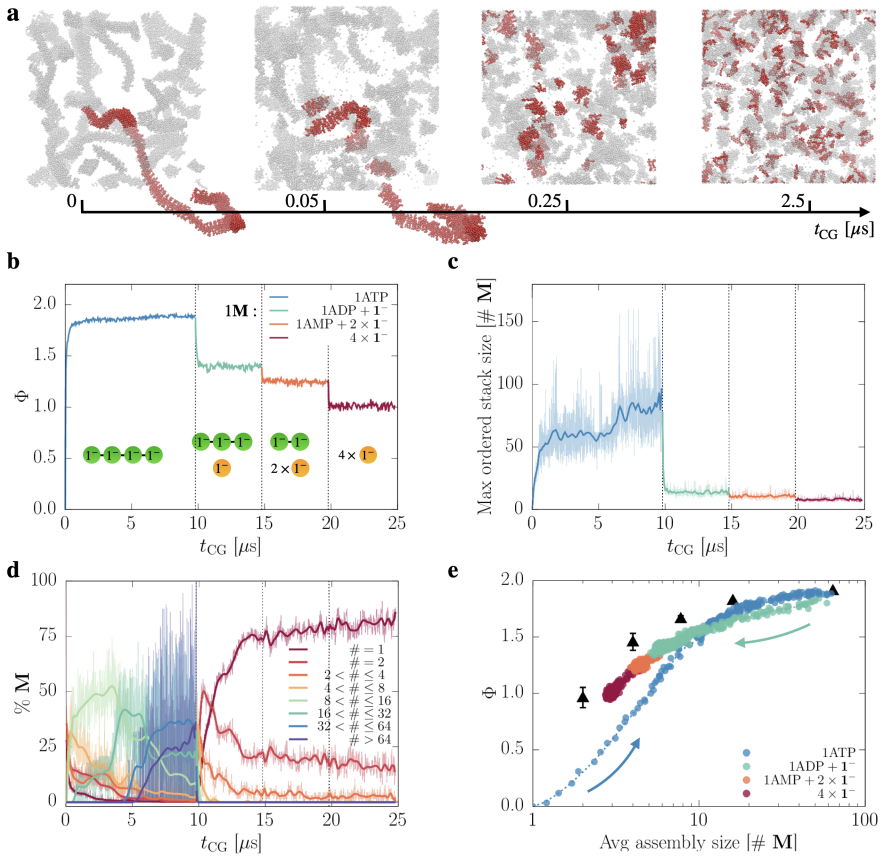

Figure 5: Disassembly triggered by successive cleavage of fuel bonds. a) Snapshots of **M** configuration taken along 2.5 μs of CG-MD after the cleavage of ATP to ADP + $\mathbf{1}^-$. The monomers highlighted in red form the largest (size= 202) ordered stack at the time of cleavage (the extended aggregate is shown in the first snapshot). b) Evolution of the order parameter (Φ). The vertical dashed lines indicate the three events of fuel cleavage, occurring at t_{CG} = 9.79, 14.79 and 19.79, shown by the cartoons. c) Evolution of the maximum size of ordered stacks (same color coding as b). d) clustering evolution of the monomers that form the longest stack at the time of first hydrolysis event (red monomers in a). e) Φ as a function of average assembly size. The black triangles indicate the Φ of pre-stacked assemblies of **M** − ATP. The arrows indicate the direction of evolution along polymerisation (blue) and depolymerisation (green).

by reproducing the effect of ATP fuel hydrolysis in a simple but effective way, i.e. statically cleaving the fuel molecules of a typical self-assembled configuration. This allowed us to observe the swift dissociation of the fibers in smaller aggregates, assessing the dynamics of its building blocks. The cluster analysis performed at the different steps of fuel dissociation demonstrated a clear variation in the time-scale of dynamical exchange among the aggregates, determined by their smaller size and by the lower cooperativity of the assembly process. This timescale difference entails an hysteresis in the path of polymerisation/depolymerisation, such that the pathway of disassembly does not overlap that of aggregate growth, providing a signature of the dissipative self-assembly process that governs the system.

The proposed model turned out to be an extremely valuable instrument to study and characterise in detail the rationale behind fuel-regulated self-assembly, opening the possibility for further extensive parametric studies, in which the main aspects of this complex phenomenon can be fully explored. The minimalistic nature of this CG model is also useful to understand the mechanisms of driven supramolecular self-assembly in general. Moreover, further simulations can be designed, e.g. by dynamically regulating the fuel composition, or by introducing competing species. This represents a step towards the rational design of biomimetic materials, by which we intend to tune the main controlling parameters of self-assembly, driving the synthesis of new materials, the properties of which could be predicted by simulations.

5 Methods

5.1 Software

All the simulations and analysis were performed with GROMACS 2018[36, 37], equipped with PLUMED 2.5[38, 39]. The parametrisation of AA models were obtained using Antechamber[40] and Gaussian 16[41]. Marvin 19.25 (ChemAxon) was used for displaying the chemical structures in Fig. 1. VMD[42] was used for visualisation and rendering of the systems in Figs. 1-5 and Table of Contents.

5.2 All-atom model

The atomistic model of **M** was built according to the General Amber Force-Field (GAFF)[43], using a bonded representation of the Zn^{2+} ions[44]. After parametrising the **M** structure without the metal ions these were included in the complex and the geometric structure was obtained by means of density functional theory optimisation, using the B3LYP functional [45, 46]. The bonded parameters of the ions were chosen consistently with Ref. [44], while the partial atomic charges were computed by means of restrained electrostatic potential (RESP) formalism [47]. ATP was parametrised using the Amber compatible

parameters of Ref. [48] and explicit water was modeled using the TIP3P representation [49].

Tha AA-MD simulations were performed integrating the equation of motion with a timestep of 2 fs. The temperature was maintained at $T = 300\,\mathrm{K}$ and the pressure at $P = 1\,\mathrm{Atm}$ by means of the V-rescale thermostat[50] and Parrinello-Rahman barostat[51] with isotropic pressure scaling, respectively. Short equilibration cycles with an integration step of 0.2 fs were performed before starting each production run.

The simulated systems were prepared by generating a pre-ordered structure of 80 **M** monomers, stacking the central benzene rings of monomers along the z axis, at 4 Å distance (see Fig. 2a), slightly larger than the equilibrium distance of 3.8 Å observed in previous AA-MD simulations[20]. In a preliminary phase the stack was equilibrated in water containing either neutralising Cl^- ions or 80 ATP molecules, randomly surrounding the fiber. During this stage, in order to avoid the dissociation of the fiber before the equilibrium conformation could be reached, we imposed a restraining potential on the center of all **M** molecules, fixing their positions to the initial one. At the same time the monomers were free to rotate along the axis of the fiber. We performed 50 ns of AA-MD applying this restraining potential, so that the **M** molecules could rearrange and find the most stable configuration, while Cl^- ions/ATP molecules were free to interact with the fiber and eventually bind to the charged Zinc ions. At the end of these 50 ns we removed the restraining potential and, after a short equilibration cycle, restarted the MD to assess the stability of the stack. To avoid the fiber from interacting with its periodic image we have selected a proper initial size of the simulation box (a $10 \times 10 \times 35\,\mathrm{nm}^3$ parallelepiped), and introduced an external wall potential acting on the center of the 1^{st}, 40^{th} and 80^{th} monomers, in order to confine their position within the simulation box, thus preventing the fiber from aligning towards the shorter sides of the box, and avoiding self-interaction.

5.3 Minimalistic model

The MD of the minimalistic model was simulated by means of the leapfrog stochastic dynamics integrator of GROMACS, with a time-step of 20 fs and an inverse friction constant $\tau_t = 100\,\mathrm{fs}$, that regulate the solvent viscosity and thermalisation of the system at $T = 300\,\mathrm{K}$. Short equilibration runs with a time-step of 5 fs were performed before the production runs. All the simulations were conducted at constant volume. For the Coulomb and van der Waals interactions a cut-off of 1.1 nm was employed, using a relative dielectric constant of $\epsilon_\mathrm{r} = 15$ to implement electro-static screening of the solvent, in analogy with the Martini force-field parameters [52].

The self-assembly systems were prepared by randomly inserting the **M** and fuel molecules in a $35 \times 35 \times 35\,\mathrm{nm}^3$ cubic box. All the self-assembly runs contained 1000 monomers, corresponding to a concentration $[\mathbf{M}] = 38.7\,\mathrm{mM}$.

Pre-stacked fibers were built by aligning the monomers with their central beads at 0.53 nm distance (the position of the minimum of the van der Waals potentials). Each newly added monomer was rotated with respect to the pre-

vious one by 180° around the fiber axis, as this was found to be the favoured configuration of ordered stacks in self-assembly simulations. The volume of the simulation box was chosen large enough to make self-interaction of the aggregate impossible. After each stack was generated, an equal number of ATP fuel molecules was randomly inserted. Similarly to the case of AA fibers, a preliminary stage of MD was performed to equilibrate the fuel with the pre-stacked fiber. In this case we have applied a restraining potential to keep the position of the central beads for 100 ns of MD. After that we performed 2 μs of dynamics without restraints to collect the results shown in Figs. 3g,5f and 5g.

5.4 Analysis

All the analysis were performed using methods and algorithms provided by GROMACS and PLUMED softwares. The `gmx clustsize` tool was used to compute the size of assemblies. Two beads at distance smaller than 0.6 nm were considered part of the same cluster. The clustering of central beads was evaluated to measure the size of fully ordered stacks, while the clustering of all **M** beads was evaluated to measure the size of generic assemblies. The radial distribution functions $\tilde{g}$ were computed by means of *gmx rdf* tool, without spherical normalisation factor, in order to make the higher order peaks more distinguishable. The average coordination number Φ was computed using PLUMED, with a coordination radius of 0.6 nm and a Fermi switching function $f(x) = (1+\beta x)^{-1}$, with $\beta = 1000$ to guarantee a sharp shift to 0 at the chosen radius.

6 Acknowledgment

The authors would like to thank Davide Bochicchio for useful discussions. The authors acknowledge funding by the Swiss National Science Foundation (SNSF grants IZLIZ2_183336) and by the European Research Council (ERC) under the European Union's Horizon 2020 research and innovation programme (grant agreement number 818776 - DYNAPOL) granted to GMP. SJG acknowledges the funding received from the Department of Biotechnology, Government of India, for the Indo-Switzerland Joint Research project (BT/IN/Swiss/55/SJG/2018-2019). The authors also acknowledge the computational resources provided by the Swiss Center for Scientific Computing (CSCS) and by CINECA.

7 Keywords

Biomimetic Materials, Fuel-driven Self-assembly, Molecular Dynamics, Molecular Modelling, Supramolecular Polymerisation.

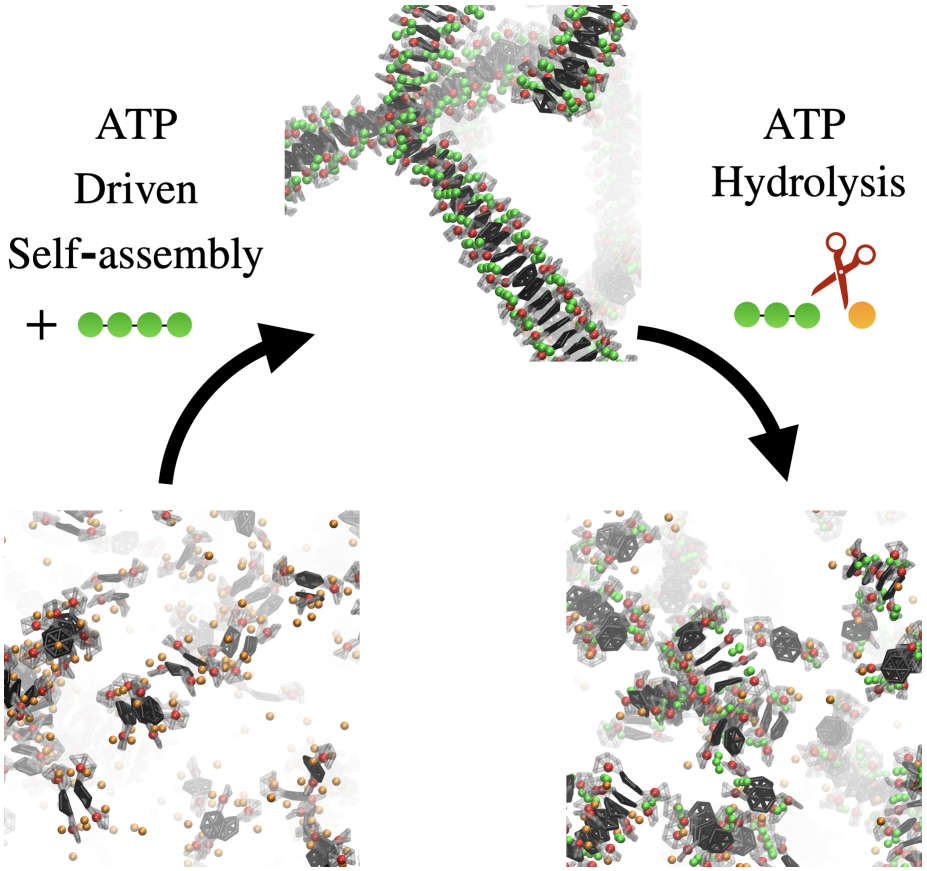

Figure 6: Molecular models provide a unique insight into the ATP-driven self-assembly and hydrolisis-triggered disassembly of fuel-regulated, bioinspired supramolecular polymers.

8 TOC

References

[1] Jean-Marie Lehn. Dynamers: dynamic molecular and supramolecular polymers. *Progress in polymer science*, 30(8-9):814–831, 2005.

[2] Anna V Davis, Robert M Yeh, and Kenneth N Raymond. Supramolecular assembly dynamics. *Proceedings of the National Academy of Sciences*, 99(8):4793–4796, 2002.

[3] T Aida, EW Meijer, and Samuel I Stupp. Functional supramolecular polymers. *Science*, 335(6070):813–817, 2012.

[4] Daan van der Zwaag, Tom FA de Greef, and EW Meijer. Programmable supramolecular polymerizations. *Angewandte Chemie International Edition*, 54(29):8334–8336, 2015.

[5] Sougata Datta, Yasuki Kato, Seiya Higashiharaguchi, Keisuke Aratsu, Atsushi Isobe, Takuho Saito, Deepak D. Prabhu, Yuichi Kitamoto, Martin J. Hollamby, Andrew J. Smith, Robert Dagleish, Najet Mahmoudi, Luca Pesce, Claudio Perego, Giovanni M. Pavan, and Shiki Yagai. Self-assembled poly-catenanes from supramolecular toroidal building blocks. *Nature*, 583(7816):400–405, July 2020.

[6] Alessandro Sorrenti, Jorge Leira-Iglesias, Akihiro Sato, and Thomas M. Hermans. Non-equilibrium steady states in supramolecular polymerization. *Nature Communications*, 8(1):15899, June 2017.

[7] Jacqui M. A. Carnall, Christopher A. Waudby, Ana M. Belenguer, Marc C. A. Stuart, Jérôme J.-P. Peyralans, and Sijbren Otto. Mechanosensitive Self-Replication Driven by Self-Organization. *Science*, 327(5972):1502–1506, March 2010.

[8] Jan W. Sadownik, Elio Mattia, Piotr Nowak, and Sijbren Otto. Diversification of self-replicating molecules. *Nature Chemistry*, 8(3):264–269, March 2016.

[9] Yinon Shafrir, Daniel ben Avraham, and Gabor Forgacs. Trafficking and signaling through the cytoskeleton: a specific mechanism. *J Cell Sci*, 113(15):2747–2757, 2000.

[10] Laura Anne Lowery and David Van Vactor. The trip of the tip: understanding the growth cone machinery. *Nature reviews Molecular cell biology*, 10(5):332, 2009.

[11] Tim Mitchison and Marc Kirschner. Dynamic instability of microtubule growth. *nature*, 312(5991):237, 1984.

[12] Michiki Kasai, Sho Asakura, and Fumio Oosawa. The cooperative nature of gf transformation of actin. *Biochimica et biophysica acta*, 57(1):22–31, 1962.

[13] Ananya Mishra, Shikha Dhiman, and Subi J. George. ATP-Driven Synthetic Supramolecular Assemblies: From ATP as a Template to Fuel. *Angewandte Chemie*, n/a(n/a), 2020.

[14] Shikha Dhiman, Ankit Jain, Mohit Kumar, and Subi J George. Adenosine-phosphate-fueled, temporally programmed supramolecular polymers with multiple transient states. *Journal of the American Chemical Society*, 139(46):16568–16575, 2017.

[15] Job Boekhoven, Wouter E Hendriksen, Ger JM Koper, Rienk Eelkema, and Jan H van Esch. Transient assembly of active materials fueled by a chemical reaction. *Science*, 349(6252):1075–1079, 2015.

[16] Soichiro Ogi, Kazunori Sugiyasu, Swarup Manna, Sadaki Samitsu, and Masayuki Takeuchi. Living supramolecular polymerization realized through a biomimetic approach. *Nature chemistry*, 6(3):188, 2014.

[17] Soichiro Ogi, Vladimir Stepanenko, Kazunori Sugiyasu, Masayuki Takeuchi, and Frank Würthner. Mechanism of self-assembly process and seeded supramolecular polymerization of perylene bisimide organogelator. *Journal of the American Chemical Society*, 137(9):3300–3307, 2015.

[18] Jiheong Kang, Daigo Miyajima, Tadashi Mori, Yoshihisa Inoue, Yoshimitsu Itoh, and Takuzo Aida. A rational strategy for the realization of chain-growth supramolecular polymerization. *Science*, 347(6222):646–651, 2015.

[19] Alessandro Aliprandi, Matteo Mauro, and Luisa De Cola. Controlling and imaging biomimetic self-assembly. *Nature chemistry*, 8(1):10, 2016.

[20] Ananya Mishra, Divya B Korlepara, Mohit Kumar, Ankit Jain, Narendra Jonnalagadda, Karteek K Bejagam, Sundaram Balasubramanian, and Subi J George. Biomimetic temporal self-assembly via fuel-driven controlled supramolecular polymerization. *Nature communications*, 9(1):1295, 2018.

[21] Ivo AW Filot, Anja RA Palmans, Peter AJ Hilbers, Rutger A van Santen, Evgeny A Pidko, and Tom FA de Greef. Understanding cooperativity in hydrogen-bond-induced supramolecular polymerization: a density functional theory study. *The Journal of Physical Chemistry B*, 114(43):13667–13674, 2010.

[22] Fatima Chami and Mark R Wilson. Molecular order in a chromonic liquid crystal: a molecular simulation study of the anionic azo dye sunset yellow. *Journal of the American Chemical Society*, 132(22):7794–7802, 2010.

[23] One-Sun Lee, Samuel I. Stupp, and George C. Schatz. Atomistic molecular dynamics simulations of peptide amphiphile self-assembly into cylindrical nanofibers. *Journal of the American Chemical Society*, 133(10):3677–3683, 2011. PMID: 21341770.

[24] Chidambar Kulkarni, Sandeep Kumar Reddy, Subi J. George, and Sundaram Balasubramanian. Cooperativity in the stacking of benzene-1,3,5-tricarboxamide: The role of dispersion. *Chemical Physics Letters*, 515(4):226 – 230, 2011.

[25] Karteek K Bejagam, Giacomo Fiorin, Michael L Klein, and Sundaram Balasubramanian. Supramolecular polymerization of benzene-1, 3, 5-tricarboxamide: a molecular dynamics simulation study. *The Journal of Physical Chemistry B*, 118(19):5218–5228, 2014.

[26] Matthew B. Baker, Lorenzo Albertazzi, Ilja K. Voets, Christianus M. A. Leenders, Anja R. A. Palmans, Giovanni M. Pavan, and E. W. Meijer. Consequences of chirality on the dynamics of a water-soluble supramolecular polymer. *Nature Communications*, 6:6234 EP –, Feb 2015. Article.

[27] Matteo Garzoni, Matthew B Baker, Christianus MA Leenders, Ilja K Voets, Lorenzo Albertazzi, Anja RA Palmans, EW Meijer, and Giovanni M Pavan. Effect of h-bonding on order amplification in the growth of a supramolecular polymer in water. *Journal of the American Chemical Society*, 138(42):13985–13995, 2016.

[28] Davide Bochicchio and Giovanni M Pavan. From cooperative self-assembly to water-soluble supramolecular polymers using coarse-grained simulations. *ACS nano*, 11(1):1000–1011, 2017.

[29] Davide Bochicchio and Giovanni M. Pavan. Effect of concentration on the supramolecular polymerization mechanism via implicit-solvent coarse-grained simulations of water-soluble 1,3,5-benzenetricarboxamide. *The Journal of Physical Chemistry Letters*, 8(16):3813–3819, 2017. PMID: 28759232.

[30] Nicolas M Casellas, Sílvia Pujals, Davide Bochicchio, Giovanni M Pavan, Tomás Torres, Lorenzo Albertazzi, and Miguel García-Iglesias. From isodesmic to highly cooperative: reverting the supramolecular polymerization mechanism in water by fine monomer design. *Chemical Communications*, 54(33):4112–4115, 2018.

[31] Sung Ho Jung, Davide Bochicchio, Giovanni M Pavan, Masayuki Takeuchi, and Kazunori Sugiyasu. A block supramolecular polymer and its kinetically enhanced stability. *Journal of the American Chemical Society*, 140(33):10570–10577, 2018.

[32] Davide Bochicchio, Matteo Salvalaglio, and Giovanni M. Pavan. Into the dynamics of a supramolecular polymer at submolecular resolution. *Nature Communications*, 8(1):147, 2017.

[33] Davide Bochicchio, Supaporn Kwangmettatam, Tibor Kudernac, and Giovanni M. Pavan. How Defects Control the Out-of-Equilibrium Dissipative Evolution of a Supramolecular Tubule. *ACS Nano*, 13(4):4322–4334, April 2019.

[34] Aritra Sarkar, Tejmani Behera, Ranjan Sasmal, Riccardo Capelli, Charly Empereur-mot, Jaladhar Mahato, Sarit S. Agasti, Giovanni M. Pavan, Arindam Chowdhury, and Subi J. George. Cooperative Supramolecular Block Copolymerization for the Synthesis of Functional Axial Organic Heterostructures. *J. Am. Chem. Soc.*, 142(26):11528–11539, July 2020.

[35] Aritra Sarkar, Ranjan Sasmal, Charly Empereur-mot, Davide Bochicchio, Srinath V. K. Kompella, Kamna Sharma, Shikha Dhiman, Balasubramanian Sundaram, Sarit S. Agasti, Giovanni M. Pavan, and Subi J.

George. Self-Sorted, Random, and Block Supramolecular Copolymers via Sequence Controlled, Multicomponent Self-Assembly. *J. Am. Chem. Soc.*, 142(16):7606–7617, April 2020.

[36] Herman JC Berendsen, David van der Spoel, and Rudi van Drunen. Gromacs: a message-passing parallel molecular dynamics implementation. *Computer physics communications*, 91(1-3):43–56, 1995.

[37] Mark James Abraham, Teemu Murtola, Roland Schulz, Szilárd Páll, Jeremy C Smith, Berk Hess, and Erik Lindahl. Gromacs: High performance molecular simulations through multi-level parallelism from laptops to supercomputers. *SoftwareX*, 1:19–25, 2015.

[38] Gareth A Tribello, Massimiliano Bonomi, Davide Branduardi, Carlo Camilloni, and Giovanni Bussi. Plumed 2: New feathers for an old bird. *Computer Physics Communications*, 185(2):604–613, 2014.

[39] The PLUMED Consortium. Promoting transparency and reproducibility in enhanced molecular simulations. *Nature Methods*, 16(8):670–673, aug 2019.

[40] Junmei Wang, Wei Wang, Peter A Kollman, and David A Case. Automatic atom type and bond type perception in molecular mechanical calculations. *Journal of molecular graphics and modelling*, 25(2):247–260, 2006.

[41] M. J. Frisch, G. W. Trucks, H. B. Schlegel, G. E. Scuseria, M. A. Robb, J. R. Cheeseman, G. Scalmani, V. Barone, G. A. Petersson, H. Nakatsuji, X. Li, M. Caricato, A. V. Marenich, J. Bloino, B. G. Janesko, R. Gomperts, B. Mennucci, H. P. Hratchian, J. V. Ortiz, A. F. Izmaylov, J. L. Sonnenberg, D. Williams-Young, F. Ding, F. Lipparini, F. Egidi, J. Goings, B. Peng, A. Petrone, T. Henderson, D. Ranasinghe, V. G. Zakrzewski, J. Gao, N. Rega, G. Zheng, W. Liang, M. Hada, M. Ehara, K. Toyota, R. Fukuda, J. Hasegawa, M. Ishida, T. Nakajima, Y. Honda, O. Kitao, H. Nakai, T. Vreven, K. Throssell, J. A. Montgomery, Jr., J. E. Peralta, F. Ogliaro, M. J. Bearpark, J. J. Heyd, E. N. Brothers, K. N. Kudin, V. N. Staroverov, T. A. Keith, R. Kobayashi, J. Normand, K. Raghavachari, A. P. Rendell, J. C. Burant, S. S. Iyengar, J. Tomasi, M. Cossi, J. M. Millam, M. Klene, C. Adamo, R. Cammi, J. W. Ochterski, R. L. Martin, K. Morokuma, O. Farkas, J. B. Foresman, and D. J. Fox. Gaussian~16 Revision C.01, 2016. Gaussian Inc. Wallingford CT.

[42] William Humphrey, Andrew Dalke, and Klaus Schulten. Vmd: visual molecular dynamics. *Journal of molecular graphics*, 14(1):33–38, 1996.

[43] Junmei Wang, Romain M. Wolf, James W. Caldwell, Peter A. Kollman, and David A. Case. Development and testing of a general amber force field. *Journal of Computational Chemistry*, 25(9):1157–1174, 2004.

[44] Zhuoqin Yu, Pengfei Li, and Kenneth M. Merz. Extended zinc amber force field (ezaff). *Journal of Chemical Theory and Computation*, 14(1):242–254, 2018. PMID: 29149560.

[45] Axel D Becke. Becke's three parameter hybrid method using the lyp correlation functional. *J. Chem. Phys*, 98:5648–5652, 1993.

[46] P. J. Stephens, F. J. Devlin, C. F. Chabalowski, and M. J. Frisch. Ab initio calculation of vibrational absorption and circular dichroism spectra using density functional force fields. *The Journal of Physical Chemistry*, 98(45):11623–11627, 1994.

[47] Christopher I. Bayly, Piotr Cieplak, Wendy Cornell, and Peter A. Kollman. A well-behaved electrostatic potential based method using charge restraints for deriving atomic charges: the resp model. *The Journal of Physical Chemistry*, 97(40):10269–10280, 1993.

[48] Kristin L. Meagher, Luke T. Redman, and Heather A. Carlson. Development of polyphosphate parameters for use with the amber force field. *Journal of Computational Chemistry*, 24(9):1016–1025, 2003.

[49] William L. Jorgensen, Jayaraman Chandrasekhar, Jeffry D. Madura, Roger W. Impey, and Michael L. Klein. Comparison of simple potential functions for simulating liquid water. *The Journal of Chemical Physics*, 79(2):926–935, 1983.

[50] Giovanni Bussi, Davide Donadio, and Michele Parrinello. Canonical sampling through velocity rescaling. *The Journal of chemical physics*, 126(1):014101, 2007.

[51] M. Parrinello and A. Rahman. Polymorphic transitions in single crystals: A new molecular dynamics method. *Journal of Applied Physics*, 52(12):7182–7190, 1981.

[52] Siewert J Marrink, H Jelger Risselada, Serge Yefimov, D Peter Tieleman, and Alex H De Vries. The martini force field: coarse grained model for biomolecular simulations. *The journal of physical chemistry B*, 111(27):7812–7824, 2007.

Supporting Information for: Multiscale Molecular Modelling of ATP-fueled Supramolecular Polymerisation and Depolymerisation

Claudio Perego[1], Luca Pesce[1], Riccardo Capelli[2], Subi J. George[3], and Giovanni M. Pavan*[1,2]

[1]Department of Innovative Technologies, University of Applied Sciences and Arts of Southern Switzerland, Galleria 2, Via Cantonale 2c, CH-6928 Manno, Switzerland
[2]Department of Applied Science and Technology, Politecnico di Torino, Corso Duca degli Abruzzi 24, 10129 Torino, Italy
[3]Supramolecular Chemistry Laboratory, New Chemistry Unit, Jawaharlal Neru Centre for Advanced Scientific Research, Jakkur, Bangalore, 560064, India

*giovanni.pavan@polito.it

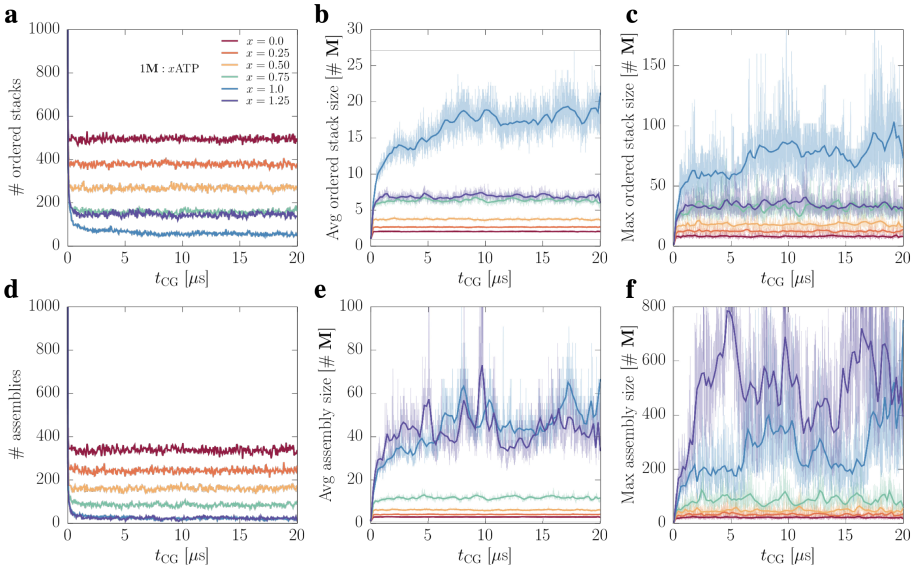

Figure S1: Self-assembly with different ATP concentrations. a) Number of ordered stacks detected versus the CG-MD time. b) Evolution of the average size of ordered stacks. The thick solid line is obtained with Bezier smoothing of the raw data (colored with 0.65 transparency). d) Evolution of the maximum size of ordered stacks. e) Number of assemblies (including disordered) detected versus the CG-MD time. d) Evolution of the average size of assemblies. d) Evolution of the maximum size of assemblies. All panels use the color coding indicated in a)

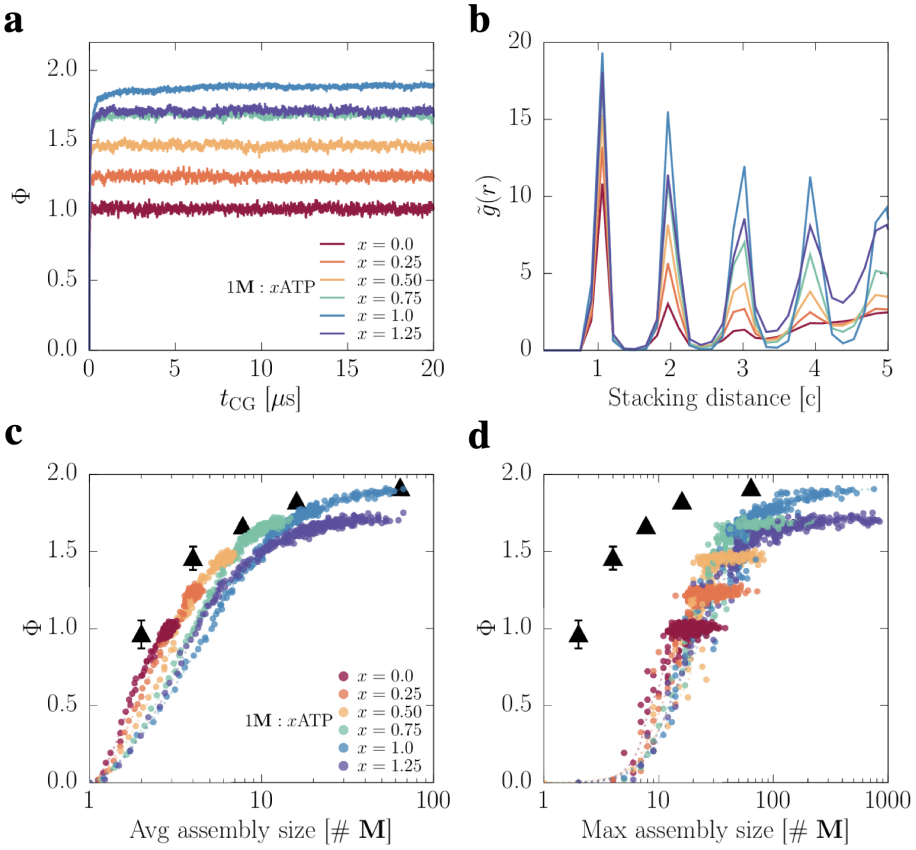

Figure S2: Ordering evolution at different ATP concentrations. a) Evolution of the order parameter Φ. b) Radial distribution function $\tilde{g}(r)$. $\tilde{g}$ is measured averaging the data from $t = 19.9\,\mu s$ to $t = 20.0\,\mu s$, and it is displayed as a function of the stacking distance $c = 0.53\,\text{nm}$. c) Φ as a function of average assembly size. The black triangles indicate the Φ of pre-stacked assemblies of $\mathbf{M}-$ATP. g) Φ as a function of maximum assembly size. The black triangles indicate the Φ of pre-stacked assemblies of $\mathbf{M}-$ATP. All panels use the color coding indicated in a)

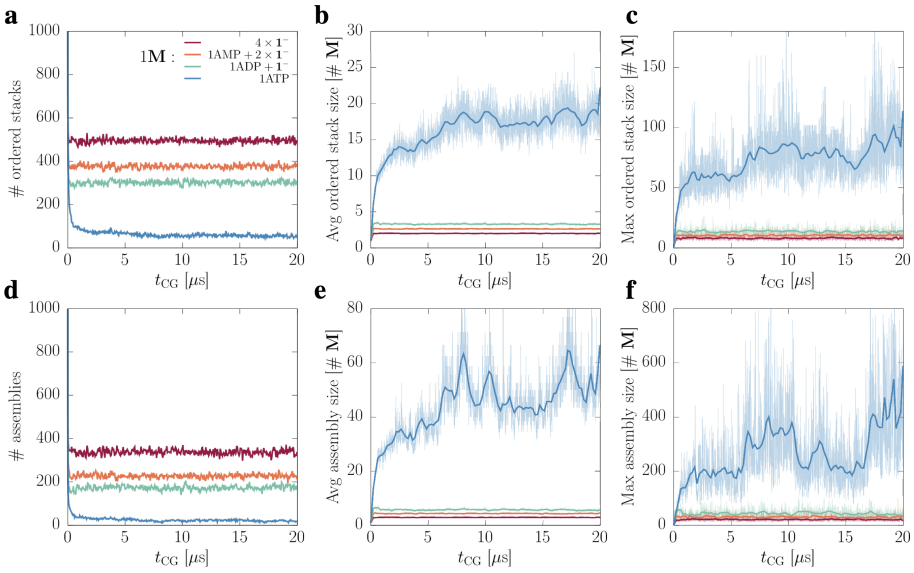

Figure S3: Self-assembly with different fuels. a) Number of ordered stacks detected versus the CG-MD time. b) Evolution of the average size of ordered stacks. The thick solid line is obtained with Bezier smoothing of the raw data (colored with 0.65 transparency). d) Evolution of the maximum size of ordered stacks. e) Number of assemblies (including disordered) detected versus the CG-MD time. d) Evolution of the average size of assemblies. d) Evolution of the maximum size of assemblies. All panels use the color coding indicated in a)

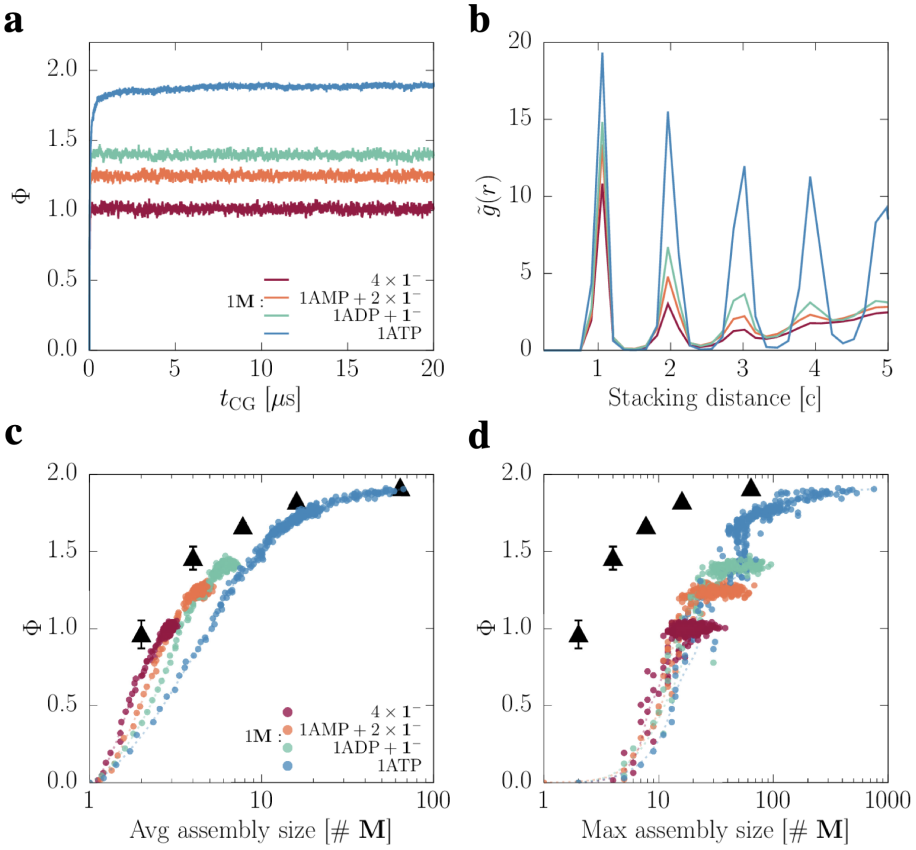

Figure S4: Ordering evolution with different fuels. a) Evolution of the order parameter Φ. b) Radial distribution function $\tilde{g}(r)$. $\tilde{g}$ is measured averaging the data from $t = 19.9\,\mu s$ to $t = 20.0\,\mu s$, and it is displayed as a function of the stacking distance $c = 0.53\,\text{nm}$. c) Φ as a function of average assembly size. The black triangles indicate the Φ of pre-stacked assemblies of $\mathbf{M} - \text{ATP}$. g) Φ as a function of maximum assembly size. The black triangles indicate the Φ of pre-stacked assemblies of $\mathbf{M} - \text{ATP}$. All panels use the color coding indicated in a)

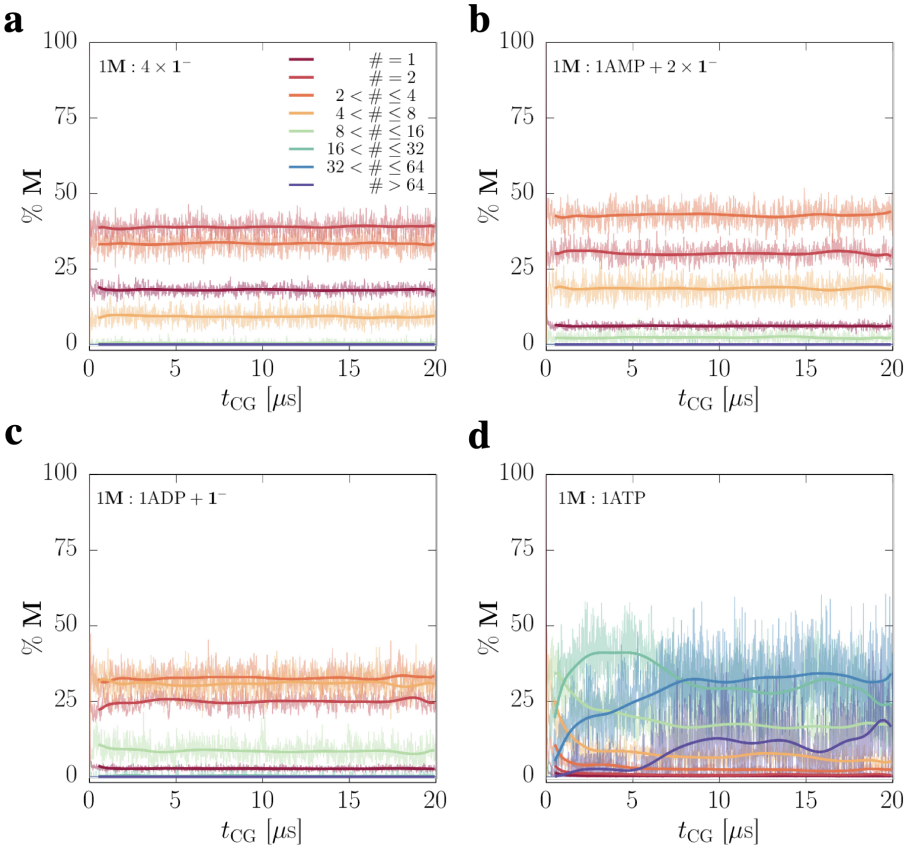

Figure S5: Sizes of ordered stacks with different fuels. Each panel shows the fraction of monomers belonging to ordered stacks of a certain size (or range of sizes) plotted vs the simulation time. The fuel composition is indicated at the upper left corner of each panel. All panels use the color coding indicated in a)

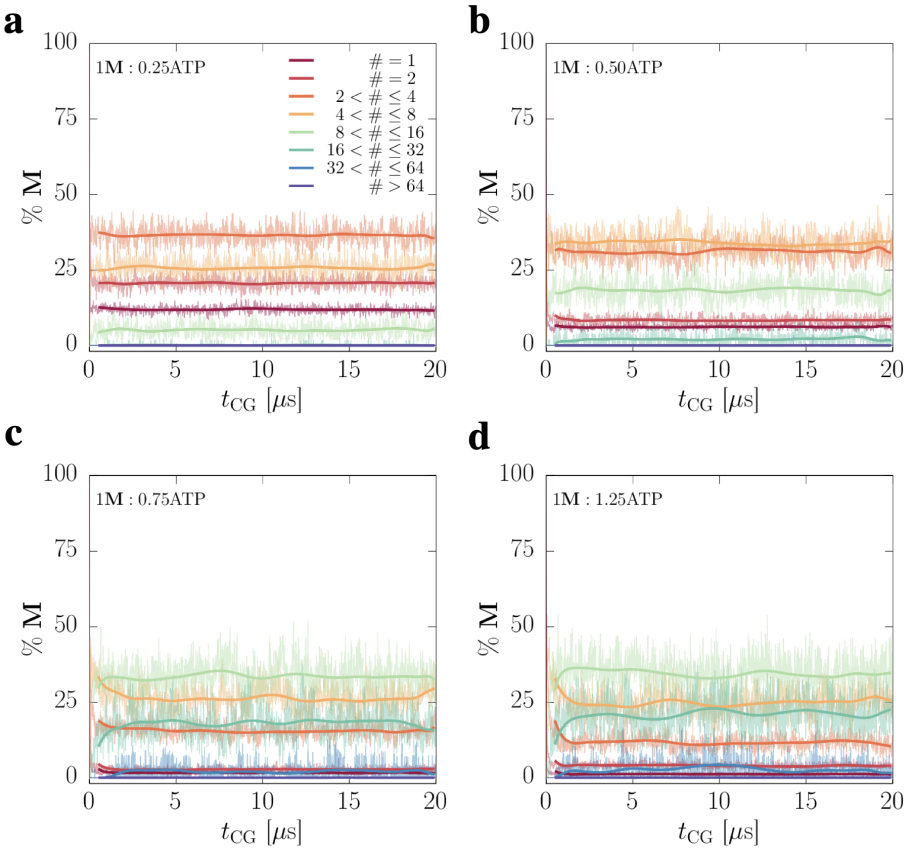

Figure S6: Sizes of ordered stacks at different ATP concentrations. Each panel shows the fraction of monomers belonging to ordered stacks of a certain size (or range of sizes) plotted vs the simulation time. The ATP concentration is indicated at the upper left corner of each panel. All panels use the color coding indicated in a)

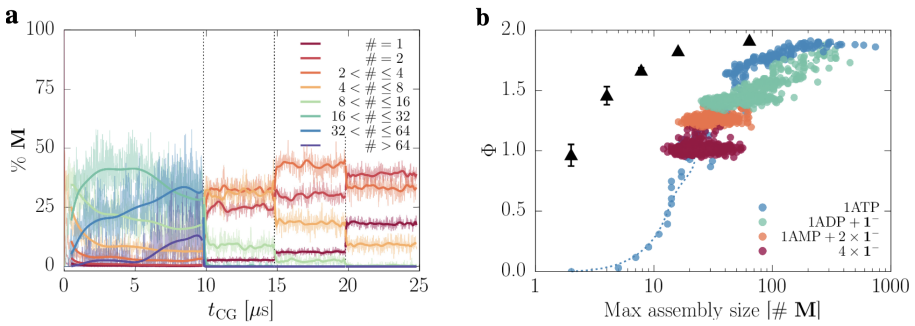

Figure S7: Disassembly triggered by successive cleavage of fuel bonds. a) fraction of monomers belonging to stacks of a certain size (or range of sizes) plotted vs the CG-MD time. The thick solid lines represent the exponential moving average (smoothed with Bezier algorithm) of the raw data (colored with 0.65 transparency). b) Φ as a function of maximum assembly size. The black triangles indicate the Φ of pre-stacked assemblies of $\mathbf{M}$ – ATP.